

Sustained Type I Interferon Reinforces NK Cell-Mediated Cancer Immunosurveillance during Chronic Virus Infection

Ji Hoon Oh¹, Myeong Joon Kim¹, Seong Jin Choi², Young Ho Ban¹, Heung Kyu Lee^{3,4}, Eui-Cheol Shin², Kyung-Mi Lee⁵, and Sang-Jun Ha¹



Abstract

The importance of natural killer (NK) cells in the early immune response to viral or bacterial infection is well known. However, the phenotype, function, and physiologic role of NK cells during the late stage of persistent viral infection have not been extensively studied. Here, we characterized NK cells in mice persistently infected with lymphocytic choriomeningitis virus clone 13 and showed that in contrast to NK cells from acutely infected or uninfected mice, NK cells from chronically infected mice expressed a terminally differentiated phenotype, stronger cytotoxicity, and reduced inhibitory

receptor expression. In an *in vivo* tumor model, chronically infected mice exhibited significantly delayed tumor progression in an NK cell-dependent manner. NK cells from chronically infected mice also expressed high STAT1, and blocking the type I interferon (IFN) receptor revealed that type I IFN signaling directly regulated NK cell cytotoxicity. Our findings indicate that sustained type I IFN signaling during chronic viral infection potentiates the cytolytic function of NK cells and contributes to NK cell-dependent host immune surveillance.

Introduction

Chronic viral infections, such as those caused by human immunodeficiency virus (HIV), hepatitis B virus, and hepatitis C virus (HCV), are global health problems. They can lead to a progressive loss of function of the host immune system (1) and an increase in the frequency of opportunistic infections (2). Although most bystander chronic viral infections negatively impact the host immune response upon subsequent infection, some persistent or latent infections may have a beneficial impact on the host immune response. For instance, coinfection of HIV with persistent GB virus C is associated with delayed HIV disease progression and reduced mortality (3, 4), and mice with latent herpes virus infection have an increased resistance to secondary *Listeria monocytogenes* or *Yersinia pestis* infections through chronic

IFN γ secretion and macrophage activation (5). Similarly, mice that are chronically infected with lymphocytic choriomeningitis virus (LCMV) are better able to clear a secondary *L. monocytogenes* infection compared with naïve mice (6). Carrier mice congenitally infected with LCMV (7) and mice infected with herpesvirus (8) exhibit potent NK cytotoxicity and resistance against tumors. Taken together, chronic viral infections can significantly modulate host immune responses to secondary pathogen infections and tumors, although the underlying mechanisms for these beneficial effects to the host have yet to be extensively elucidated.

Type I IFNs, including IFN α and IFN β , are secreted during the early stages of a viral infection and play differential roles in acute and chronic infections (9). During chronic viral infection, type I IFNs typically play an immunosuppressive role rather than the classic antiviral role. Several studies have shown that blockade of type I IFN signaling during chronic viral infection decreases IL10 production and programmed death-ligand 1 (PD-L1) expression in dendritic cells, resulting in enhanced virus-specific CD4⁺ T-cell responses and virus control (10, 11). Long-term administration of IFN α to naïve mice was shown to inhibit CD8⁺ T-cell responses through the accumulation and activation of myeloid-derived suppressor cells (12).

Welsh and colleagues were the first to identify an NK cell response to LCMV-infected mice that peaked between days 3 and 5 after infection (13). Subsequent studies have revealed that NK cells play a significant role as regulators of the T-cell responses to LCMV infection. In the early stages of chronic viral infection, NK cells activated by type I IFNs inhibit T-cell-mediated pathology by promoting T-cell exhaustion and death (14). Numerous studies have found that depletion of NK cells before or at the time of infection can lead to hyperactivation of virus-specific T-cell responses and host death (15, 16), demonstrating that NK cells play a critical immunosuppressive role during early chronic viral infection. In contrast, one study has reported that T-cell-mediated pathology did not occur when NK cells were eliminated at the late

¹Department of Biochemistry, College of Life Science and Biotechnology, Yonsei University, Seoul, Republic of Korea. ²Laboratory of Immunology and Infectious Diseases, Graduate School of Medical Science and Engineering, KAIST, Daejeon, Republic of Korea. ³Laboratory of Host Defenses, Graduate School of Medical Science and Engineering, Korea Advanced Institute of Science and Technology, Daejeon, Republic of Korea. ⁴Biomedical Science and Engineering Interdisciplinary Program, Korea Advanced Institute of Science and Technology, Daejeon, Republic of Korea. ⁵Department of Biochemistry and Molecular Biology, Korea University College of Medicine, Seoul, Republic of Korea.

Note: Supplementary data for this article are available at Cancer Immunology Research Online (<http://cancerimmunolres.aacrjournals.org/>).

Corresponding Authors: Sang-Jun Ha, Yonsei University, 50 Yonsei-ro, Seodaemun-gu, Seoul 03722, Republic of Korea. Phone: 82-2-2123-2696; Fax: 82-2-362-9897; E-mail: sjha@yonsei.ac.kr; and Kyung-Mi Lee, Department of Biochemistry and Molecular Biology, Korea University College of Medicine, Seoul 02841, Republic of Korea. Phone: 82-2-2286-1300; Fax: 82-2-920-6252; E-mail: kyunglee@korea.ac.kr

doi: 10.1158/2326-6066.CIR-18-0403

©2019 American Association for Cancer Research.

stage of chronic LCMV infection (17). Clearly, NK cells play distinct roles at different stages of chronic viral infections. However, the specific details of these roles and the underlying mechanisms have yet to be determined. To address this issue, we analyzed the phenotype and activation mechanism of NK cells in mice after establishment of severe chronic viral infection. Chronically infected mice exhibited increased NK cell maturation and cytotoxic activity and enhanced antitumor immunity compared with naïve mice, and these effects were due, in part, to type I IFN signaling. Taken together, the data suggest that type I IFNs play a typical immunosuppressive role in the late phase of chronic viral infection, but also enhance the cytotoxicity of NK cells to improve immune surveillance against tumors.

Materials and Methods

Mice

Five- to 6-week-old female C57BL/6 mice were purchased from the Jackson Laboratory. All purchased mice were allowed to acclimate to our animal facility environment for a minimum of 2 weeks before using experiments. Ly5.1⁺ and IFNAR1^{-/-} mice were obtained from Prof. Young-Chul Sung (POSTECH, Pohang, Korea) and Prof. Heung Kyu Lee (KAIST, Daejeon, Korea). For adoptive transfer experiments, wild-type (WT) mice were bred onto homozygous Ly5.1-allele backgrounds for two generations before using in experiments. Sex- and age-matched mice were randomly assigned to experiments. All mice were maintained in a specific pathogen-free facility at Yonsei University. All animal experiments were performed in accordance with the Korean Food and Drug Administration guidelines. Protocols were reviewed and approved by the Institutional Animal Care and Use Committee (IACUC) of Yonsei University (permit number: IACUC-A-201507-352-01).

Cell culture

B16F10 mouse melanoma cells were obtained from ATCC in 2010 and were cultured in complete Dulbecco's modified Eagle's medium (DMEM) consisting of 10% FBS (GE Healthcare UK Ltd) and 1% penicillin/streptomycin (Gibco Laboratories). TC-1 lung adenocarcinoma cells were obtained from ATCC in 2010 and were cultured in complete Roswell Park Memorial Institute (RPMI) consisting of 10% FBS and 1% penicillin/streptomycin. Vero monkey kidney cells were obtained from ATCC in 2009 and were cultured in complete DMEM consisting of 10% FBS and 1% penicillin/streptomycin. YAC-1 mouse lymphoma cells were obtained from ATCC in 2009 and were cultured in complete RPMI consisting of 10% FBS and 1% penicillin/streptomycin. EG7 thymoma cells were kindly provided by Prof. Jun Chang (Ewha Womans University, Seoul, Korea) and were cultured in complete RPMI consisting of 10% FBS and 1% penicillin/streptomycin. Tumor cells were tested yearly for *Mycoplasma* contamination using the e-Myco Mycoplasma PCR Detection Kit (iNtRON Biotechnology) and reauthentication was not performed in the past years. Cells were maintained at 37°C in humidified air with 5% CO₂ and used *in vivo* or *in vitro* experiment after 2 to 3 passages.

LCMV infection

LCMV-clone 13 (Cl13), a variant derived from an LCMV-Armstrong (Arm) CA1371 carrier mouse, was obtained from Dr. Rafi Ahmed (Emory Vaccine Center, Atlanta, GA). Eight-

week-old female mice were infected with 2×10^5 plaque-forming units (PFU) of LCMV-Arm diluted in 500 μ L of serum-free RPMI medium by intraperitoneal (i.p.) infection or with 2×10^6 PFU of LCMV-Cl13 diluted in 500 μ L of serum-free RPMI medium by intravenous (i.v.) infection. For most chronic infections, mice were injected i.p. with 0.2 mg of anti-CD4 for CD4⁺ T-cell depletion (GK1.5; Bio X Cell) on days -1 and 0 relative to infection with LCMV-Cl13 on day 0. The mice infected with Cl13 after depletion of CD4⁺ T cells are labeled "Cl13" in most figures except for Fig. 4, where it is specifically labeled "Cl13 (with α CD4)" to distinguish it from the other groups. In this figure, mice in the group labeled "Cl13 (w/o α CD4)" were infected with LCMV-Cl13 without receiving the CD4 depletion antibody.

For virus titration, three to five drops of blood were collected from the retro-orbital sinus at the indicated time points, and the serum was immediately stored at -70°C. Spleens or tumors from LCMV-infected mice at the indicated time points were harvested, weighed, homogenized (30 seconds at 20,000 rpm; Polytron PT10-35 homogenizer, Kinematica) in 1 mL of DMEM consisting of 1% FBS and 1% penicillin/streptomycin and stored at -70°C. Viral titers from serum or homogenized tissue samples were determined by plaque assay on Vero cells as previously described (18). Briefly, 3.5×10^5 Vero cells were plated in 35-mm wells in 6-well dishes (Costar) and the plates were incubated at 37°C. When the cell monolayers were confluent, the medium was removed, and titrated amounts of serum or homogenized tissue samples (in a total volume of 200 μ L) were added to the cells. After adsorption for 1 hour at 37°C, the cells were overlaid with 4 mL of 1% agarose (SeaKem GTG agarose; Lonza) in Medium 199 (Gibco Laboratories) supplemented with 10% FBS, 1% penicillin/streptomycin, and L-glutamine (Gibco Laboratories). The plates were incubated for 4 days at 37°C and then overlaid with 3 mL of 1% agarose in Medium 199 containing 1% neutral red (Thermo Fisher Scientific). Plaques were counted the following day. The detection limit (one plaque in the well) is 50 PFU/mL indicated by a dashed line. The undetectable samples were given a value of 20 PFU for display on the graph.

Cell preparation for analysis

Lymphocytes from bone marrow, spleen, peripheral blood, and lungs were isolated as previously described (19). Bone marrow cells were isolated from femurs of mice. Spleens were mashed through a 70- μ m cell strainer (BD Falcon), and red blood cell (RBC) lysis was performed using ACK lysing buffer (Gibco Laboratories). Peripheral blood was obtained from the retro-orbital sinus using heparinized capillary tubes (Marienfeld), and peripheral blood mononuclear cells were purified via density-gradient centrifugation method using Histopaque-1077 (Sigma-Aldrich). Pulmonary lymphocytes were obtained from PBS-perfused whole lung. Lung tissue was harvested, chopped, digested with type II collagenase (1 mg/mL; Worthington Biochemical Corp.) and DNase I (0.01 mg/mL; Sigma-Aldrich) for 1 hour at 37°C on a shaking incubator at 250 rpm, and filtered through a 70- μ m cell strainer (BD Falcon). Lymphocytes were enriched by Percoll (Sigma-Aldrich) density-gradient centrifugation and collected from the interface of the 44% and 67% Percoll layers. To isolate tumor-infiltrating lymphocytes (TIL), tumors were harvested, weighed, diced, and digested in RPMI consisting of 10% FBS, 1% penicillin/streptomycin, type IV collagenase (1 mg/mL; Worthington Biochemical Corp.), and DNase I (0.01 mg/mL; Sigma-Aldrich) for 30 minutes at 37°C on a shaking

incubator at 250 rpm. After digestion, tumors were filtered through a 70- μ m cell strainer (BD Falcon), and RBC lysis was performed using ACK lysing buffer (Gibco Laboratories). After washing with RPMI consisting of 2% FBS and 1% penicillin/streptomycin, cells were counted using hemocytometer.

Flow cytometry analysis

For phenotypic analysis of lymphocytes, single-cell suspensions were plated at 10^6 cells/well in 96-well plates (round-bottom) in PBS consisting of 2% FBS and were stained with fluorochrome-conjugated antibodies for 20 minutes in 4°C. Antibodies against CD3 (145-2C11), CD4 (RM4-5), CD11b (M1/70), CD27 (LG.3A10), CD45.1 (A20), CD69 (H1.2F3), CD314 (CX5), Ly49C/I (5E6), CD107a (1D4B), IFN γ (XMG1.2), and NK1.1 (PK136) were from BD Biosciences; antibodies against CD8a (53-6.7), CD45.2 (104), T-bet (ebio4B10), CD16/32 (93), and TNF α (MP6-XT22) were from eBioscience; and antibodies against CD43 (1B11), CD49b (DX5), CD335 (29A1.4), granzyme B (GB11), KLRG1 (2F1), NKG2A (16A11), LFA-1 (H155-78), DNAM-1 (10E5), and IL2 (JES6-5H4) were from BioLegend. To measure the proliferation capability *ex vivo*, lymphocytes (10^6 cells/well) from bone marrow, spleen, or lungs were stained with a Ki-67 antibody (B56; BD Biosciences). For analysis of apoptosis *ex vivo* or *in vitro*, lymphocytes from bone marrow, spleen, or lungs or purified NK cells from spleen were incubated with Annexin V and 7AAD (BD Biosciences), according to the manufacturer's protocol. Anti-CD16/32 mAb (93; eBioscience) was used to block Fc γ receptors prior to surface staining, except for CD16/32 staining. The LIVE/DEAD fixable dead cell stain kit (Invitrogen) was used to remove the dead cell population in most staining procedures, except for apoptosis staining, according to the manufacturer's instructions.

To determine the functions of NK cells *in vitro*, lymphocytes (1.5×10^6 cells/well) from spleen or lungs were incubated with both recombinant (r)IL12 (5 ng/mL; R&D Systems) and rIL18 (5 ng/mL; R&D Systems) or YAC-1 cells (E:T ratio: 10:1) in the presence of GolgiPlug (1 μ g/mL; BD Biosciences), GolgiStop (3 μ mol/L; BD Biosciences), and anti-CD107a (5 μ g/mL; BD Biosciences) at 37°C for 5 hours, followed by intracellular cytokine staining using an anti-IFN γ . In case of detection of IFN γ in NK cells from tumors, NK cells were stimulated with precoated plate-bound activating anti-NK1.1 (2 μ g/mL; clone PK136; BioLegend) at 37°C for 5 hours.

To detect degranulation and intracellular cytokines in T cells from spleen and tumor, splenocytes, and TILs were incubated with LCMV-glycoprotein (GP) peptide mixture containing GP₃₃₋₄₁ (0.2 μ g/mL), GP₂₇₆₋₂₈₆ (0.2 μ g/mL), and GP₆₆₋₈₀ (5 μ g/mL) peptides, or ovalbumin (OVA) peptide mixture containing OVA₂₅₇₋₂₆₄ (0.2 μ g/mL) and OVA₃₂₃₋₃₃₉ (5 μ g/mL) peptides in the presence of GolgiPlug (1 μ g/mL; BD Biosciences), GolgiStop (3 μ mol/L; BD Biosciences), and anti-CD107a (5 μ g/mL; BD Biosciences) at 37°C for 5 hours, followed by intracellular cytokine staining using anti-IL2, anti-TNF α , and anti-IFN γ antibodies. All peptides were synthesized by GenScript, respectively at a purity >95%.

Intracellular staining was performed after surface staining using the BD Cytofix/Cytoperm fixation/permeabilization kit (BD Biosciences) or the Foxp3/transcription factor staining buffer set (eBioscience), according to the manufacturer's instructions. All stained samples were analyzed on a FACSCanto II instrument (BD Biosciences) and analyzed using FlowJo software (Tree Star).

To characterize the NK cells and T cells, lymphocyte populations were gated based on forward scatter (FSC)-A and side scatter (SSC)-A. FSC-H and FSC-A were used for doublet exclusion. Dead cells were then gated out of the lymphocytes and then gated by NK1.1, CD4, or CD8 versus CD3. The NK cells, CD4⁺ T cells, and CD8⁺ T cells were defined as NK1.1⁺CD3⁻ cells, NK1.1⁻CD3⁺CD4⁺ cells, and NK1.1⁻CD3⁺CD8⁺ cells, respectively. The immature NK cells were defined as NK1.1⁺CD27^{low}CD11b^{low}, NK1.1⁺CD27^{high}CD11b^{low}, NK1.1⁺CD27^{high}CD11b^{low}, and NK1.1⁺CD11b^{high}KLRG1^{low} cells, and mature NK cells were defined as NK1.1⁺CD27^{low}CD11b^{high} and NK1.1⁺CD11b^{high}KLRG1^{high} cells.

Signaling molecule staining

All immunostaining experiments were performed as previously described (20). To assess total intracellular STAT1, splenocytes (2×10^6 cells/well) were stained with fluorescein isothiocyanate-conjugated anti-NK1.1 (BD Biosciences), fixed, and permeabilized with Cytofix/Cytoperm (BD Biosciences), prechilled (kept at -20°C for 2 hours) pure methanol, and then stained with PerCP-Cy5.5-conjugated anti-CD3 (BD Biosciences) and Alexa Fluor 647-conjugated anti-STAT1 (1/Stat1, BD Biosciences) or mouse IgG1 isotype control (MOPC-21; BioLegend). For phosphorylation studies, splenocytes (2×10^6 cells/well) were incubated for 4 hours at 37°C to clear receptors of cytokines bound *in vivo* and to allow the cells to return to baseline before stimulation with IFN β (50,000 U/mL; R&D Systems) and IFN γ (100 ng/mL; R&D Systems) for STAT1 phosphorylation or IFN β (50,000 U/mL) and IL12 (200 ng/mL; R&D Systems) for STAT4 phosphorylation. Splenocytes were then incubated with the previously mentioned cytokines at 37°C for 90 minutes and collected for intracellular staining of pSTAT1 and pSTAT4. Intracellular pSTAT protein was stained with brilliant violet (BV) 421-conjugated anti-pSTAT1 pY701 (4a; BD Biosciences) or the corresponding isotype control, BV421-conjugated mouse IgG2a (MOPC-173; BioLegend), and PE-conjugated anti-pSTAT4 pY693(38/p-Stat4; BD Biosciences) or the corresponding isotype control, PE-conjugated mouse IgG2b (MPC-11; BioLegend).

In vitro cytotoxicity assay

In vitro cytotoxicity was analyzed by flow cytometry as previously described (21). Briefly, YAC-1 target cells (10^4 cells) were labeled with 2×10^{-6} mol/L PKH26 dye (Sigma-Aldrich) and cultured in quadruplicate at different E:T ratios (5:1, 10:1, and 20:1) of NK cells purified from the lungs of uninfected or LCMV-Cl13-infected mice. After 4 hours, the cells were stained with the viability probe TO-PRO-3 iodide (Invitrogen), and cytotoxicity was determined by flow cytometry as the percentage of dead YAC-1 cells (PKH26⁺ TO-PRO-3⁺). The proportion of spontaneous dead YAC-1 cells never exceeded 6%.

Analysis of cytokine secretion *in vivo*

Sera were obtained from uninfected and LCMV-Cl13-infected mice at 41 days post infection (dpi) and were diluted at 1:2 with sample diluent for cytokine measurement. IL15 and IL18 concentrations were measured using the Mouse IL15/15R Platinum ELISA kit (eBioscience) and Mouse IL18 Platinum ELISA kit (eBioscience), and other cytokines were measured using the LEGENDplex Multi-Analyte Flow Assay Kit (BioLegend) according to the manufacturer's instructions.

Cell sorting, RNA isolation, and qRT-PCR

Splenocytes (1.2×10^9 cells/group) from uninfected, LCMV-Arm-immune (>40 days after LCMV-Arm infection), or LCMV-Cl13-infected mice digested with type II collagenase (1 mg/mL; Worthington Biochemical Corp.) and DNase I (50 U/mL; Sigma-Aldrich) were incubated with a cocktail of biotin-conjugated antibodies and antibiotin beads (Miltenyi Biotech) and were subsequently depleted of T cells with CD90.2 Microbeads ($10 \mu\text{L}/10^7$ cells; Miltenyi Biotech) and B cells with CD19 Microbeads ($10 \mu\text{L}/10^7$ cells; Miltenyi Biotech). After depletion, cells were stained with CD3 and NK1.1 antibodies for sorting of NK cells (NK1.1⁺CD3⁻). The stained cells were sorted using a FACSAria II instrument (BD Biosciences). The purity of the cells after sorting was >98%.

Total RNA was extracted using an RNeasyPlus micro kit (Qiagen), and the concentration and purity of RNA were measured using the Nanodrop 1000 spectrophotometer (Thermo Scientific). Total RNA (500 ng) was used to synthesize cDNA using reverse transcription using a transcript first-strand cDNA synthesis kit (Roche) according to the manufacturer's instructions. The expression of individual genes was measured in triplicate by qPCR on a CFX96 real-time PCR detection system (Bio-Rad) with the following gene-specific forward (F) and reverse (R) primers: *Stat1* F: TCACAGTGGTTCGAGCTTCAG and R: CGAGACATCATAGGCAGCGTG; *Stat2* F: GTTACACCAGTCTACTCACAGA and R: TGGTCTTCAATCCAGGTAGCC; *Stat3* F: CACCTTGGATTGAGAGTCAAGAC and R: AGAATCGGCTATATTGCTGGT; *Stat4* F: TGGCAACAATTCTGCTTCAAAAC and R: GAGGTCCTGGATAGGCATGT; *Stat5a* F: CGCCAGATGCAAGTGTGTAT and R: TCCTGGGGATTATCCAAGTCAAT; *Stat5b* F: CGATGCCCTTACCAGATG and R: AGCTGGGTGGCCTTAATGTTC; *Stat6* F: CTCGTGGGGCCTAATTTCCA and R: GCATCTGAACCGACCAGGAAC; and *Gapdh* F: AGGTCGGTGTGAACGGATTT and R: TGTAGACCATGTAGTTGAGG (22). qPCR reaction conditions were as follows: after initial denaturation of the template for 5 minutes at 95°C, 50 thermal cycles of 15 seconds at 95°C, 20 seconds at 60°C, and 30 seconds at 72°C were performed in a final volume of 20 μL using SYBR Green I dye for PCR-product detection (Qiagen) according to the manufacturer's instructions. Relative mRNA expression was normalized to *Gapdh* expression and calculated according to the $\Delta\Delta\text{CT}$ method.

Adoptive cell transfer

For transfer experiments, congenically marked (Ly5.1/5.1) splenocytes (4×10^6 cells/mouse) from naïve WT mice were transferred i.p. into uninfected or LCMV-Cl13-infected mice (Ly5.2/5.2), respectively. After 3 days, transferred cells were recovered by peritoneal lavage and analyzed for granzyme B (GzmB)⁺ NK cells.

For cotransfer experiments, uninfected or LCMV-Cl13-infected WT mice (Ly5.1/5.1) were injected i.v. with a 1:1 mixture of 2×10^6 splenocytes from naïve WT (Ly5.1/5.2) and naïve IFNAR1^{-/-} (Ly5.2/5.2) mice. After 3 days, transferred cells from spleen of the recipients were analyzed for STAT1⁺ and GzmB⁺ NK cells.

In vivo blockade of type I IFN signaling

To block type I IFN signaling *in vivo*, 0.5 mg of anti-IFNAR1 (MAR1-5A3; Bio X Cell) or mouse IgG1 isotype control (MOPC-21; Bio X Cell) was administered to LCMV-Cl13-infected mice at days 0 and 1 by i.v. injection. Five days after primary injection of blocking antibodies, mice were sacrificed, and NK

cells harvested from the spleen and lungs and were analyzed using flow cytometry.

Tumor experiments

For tumor metastasis models, mice were i.v. injected with B16F10 (5×10^5 cells/mouse) or TC-1 (5×10^5 cells/mouse) tumor cells into the tail vein. Mice were euthanized, and their lungs were harvested at days 17 or 21 after tumor injection. The total number of visible nodules on both lungs and on one lobe of the lungs was counted. For survival experiments, tumor-injected mice were monitored daily until death or appearance of moribund symptoms, such as lethargy, weight loss, and a hunched back. In some experiments, LCMV-Cl13-infected mice were injected i.v. with depleting antibodies (Bio X Cell) against CD4 (GK1.5), CD8 (2.43), or NK1.1 (PK136), as well as IFNAR1-blocking antibody (MAR1-5A3) 4 days before B16F10 or TC-1 tumor injection (day -4; 1 mg) and at days 5 (0.5 mg) and 15 (0.5 mg) after tumor injection. Control groups were injected with PBS or isotype-control antibodies, and depletion efficacy was confirmed in the bone marrow, spleen, and lungs by flow cytometry 17 days after antibody administration. For subcutaneous tumor models, B16F10, TC-1, or EG7 tumor cells resuspended in 100 μL of PBS were injected subcutaneously in the shaved left flank. Tumor growth was monitored every 3 to 4 days by measuring the tumor size using a caliper, and tumor volume was calculated as length \times width² \times 0.5. Mice were euthanized when tumors reached 15 mm in diameter.

In vitro cell viability assay after LCMV infection

TC-1, B16F10, or EG7 tumor cells (1×10^5 cells/well) were plated at a 6-well plate in 3 mL of the corresponding tumor cell culture medium on day -1. On day 0, the medium was removed and then cells were infected with different multiplicity of infection of LCMV-Cl13 (500 μL per well) for 1 hour at 37°C. After 1 hour, 2.5 mL of culture medium was added. On day 1, cells were harvested and viability was evaluated using Trypan blue staining.

Statistical analysis

Statistical analysis was performed using Prism software version 5.02 (GraphPad). Significant differences between groups were analyzed by two-tailed unpaired Student *t* test or one-way ANOVA with *post hoc* Tukey test or Dunnett test for multiple comparison. Kaplan-Meier survival curves were analyzed using Mantel-Cox log-rank test with a 95% CI. *P* < 0.05 was considered statistically significant.

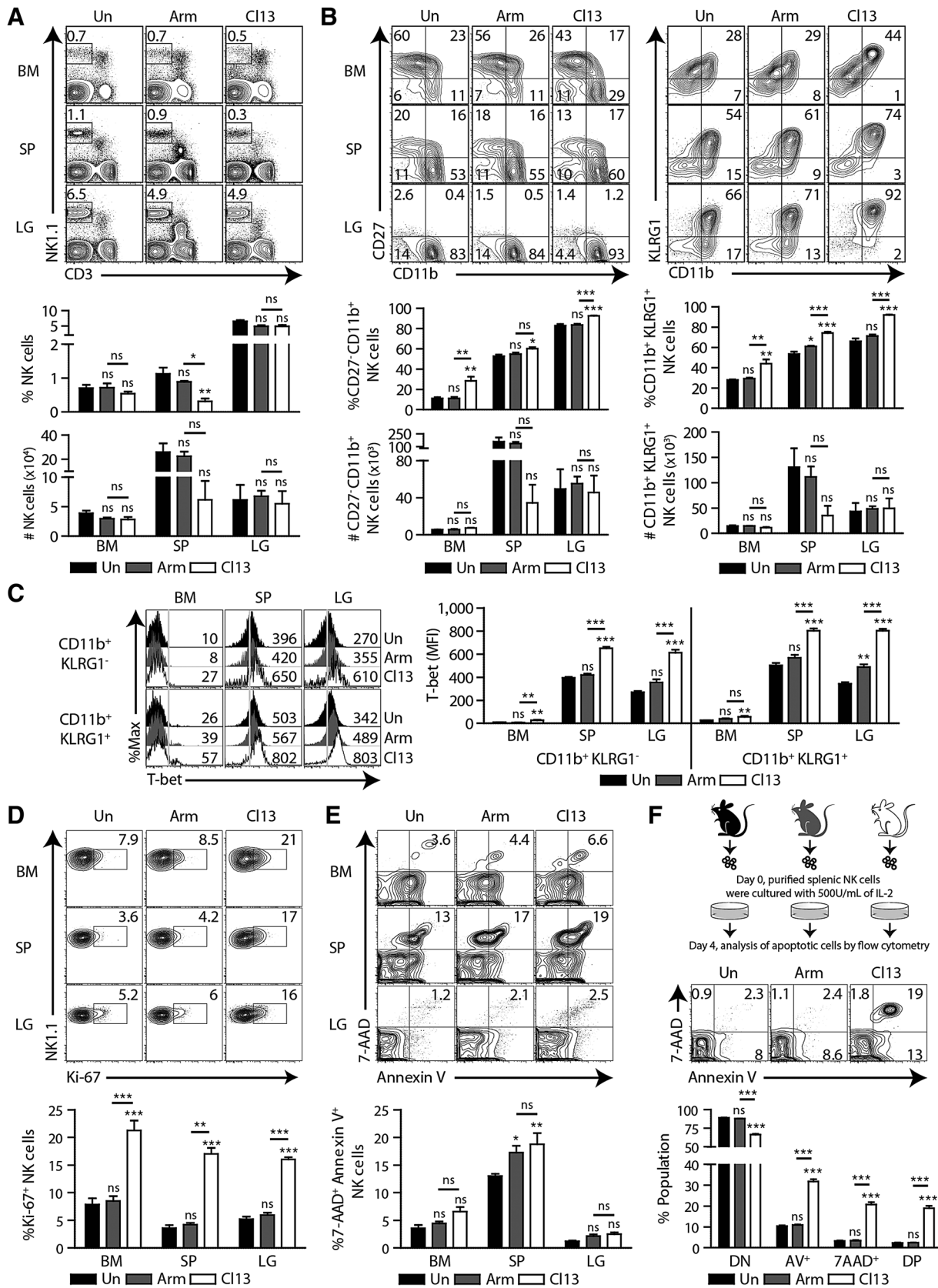
Results

Chronic LCMV infection results in a decreased population of mature NK cells

To investigate the role of NK cells after establishment of chronic viral infection, we used a previously described murine model of chronic, uncontrolled LCMV-Cl13 (Cl13) infection (23). In this model, CD4⁺ T cells were temporarily depleted with anti-CD4 prior to infection with Cl13, resulting in a systemic and life-long chronic infection. CD4⁺ T-cell numbers returned to similar levels to naïve mice within 30 dpi. A control group of mice was acutely infected with LCMV-Armstrong (Arm) resulting in peak viral titers at 3 dpi and complete viral clearance by 8 dpi.

We analyzed bone marrow and peripheral NK cells from uninfected mice, LCMV-Arm-immunized mice (40 dpi), and

Oh et al.



Cl13-infected mice (40 dpi). Compared with uninfected or LCMV-Arm-immunized mice, Cl13-infected mice had lower frequencies of CD3⁺NK1.1⁺ NK cells in the spleen, but not in the bone marrow or lungs (Fig. 1A). However, the frequencies of mature CD27^{low}CD11b^{high} and terminally differentiated CD11b^{high}KLRG1⁺ NK cells were higher in Cl13-infected mice than in uninfected or LCMV-Arm-immunized mice (Fig. 1B). These frequencies were still higher in mice at 53 and 69 days after establishment of chronic virus infection than in uninfected mice (Supplementary Fig. S1A). A significant upregulation of T-bet, a key transcription factor involved in NK cell development, was also observed in both immature and mature NK cells of Cl13-infected mice (Fig. 1C). NK cells from Cl13-infected mice displayed 2- to 3-fold increase in proliferation (compared with cells from uninfected or LCMV-Arm-immunized controls; Fig. 1D). Collectively, these data suggested that chronic LCMV infection promoted NK cell maturation and proliferation.

To determine why fewer NK cells in Cl13-infected mice were seen, we assessed their apoptotic status by flow cytometry. A higher percentage of NK cells were apoptotic (Annexin V⁺7AAD⁺) in the spleens Cl13-infected mice compared with uninfected controls (Fig. 1E). This effect was amplified when splenic NK cells were purified and cultured with IL2 for 4 days (Fig. 1F). These data suggested that NK cells from Cl13-infected mice were more proliferative, but apoptotic during chronic LCMV infection. Taken together, although the maturity of NK cells in Cl13-infected mice increased, the number of mature NK cells decreased due to accelerated proliferation and apoptosis.

NK cells display an activated phenotype and increased cytotoxicity during chronic infection

Several studies have reported that terminally differentiated NK cells display strong effector functions (24). Because NK cell activation is determined by the integration of activating and inhibitory signals (25), we analyzed the expression of activating and inhibitory receptors. NK cells in Cl13-infected mice expressed the activating receptors, CD16, lymphocyte function-associated antigen 1 (LFA-1), and NKG2D similarly to those from uninfected or Arm-immunized mice, with the exception of higher activating receptor NKG2D expression in bone marrow (Fig. 2A). In contrast, the surface expression of inhibitory receptors [Ly49C/I and NKG2A; specific for self major histocompatibility complex (MHC) class I] was significantly lower in NK cells from Cl13-infected mice than in those from uninfected or Arm-immunized mice (Fig. 2B). Consistent with the fact that NK cell function is regulated by the balanced expression of activating and inhibitory

receptors, expression of the early activation marker CD69 and cytotoxic granzyme B (GzmB) was significantly elevated in NK cells from Cl13-infected mice (Fig. 2C). These phenotypes were also observed at various time points in mice after establishment of chronic virus infection (Supplementary Fig. S1B and S1C). Collectively, these data indicated that decreased inhibitory receptor expression on NK cells during chronic virus infection lowered the threshold necessary for activation of the cells.

To assess the functional capacity of NK cells from chronically infected mice, IFN γ production and cytotoxicity were measured following stimulation with inflammatory cytokines. NK cells from Cl13-infected mice produced fewer IFN γ than uninfected mice (Supplementary Fig. S2), but displayed an increase in CD107a expression and IFN γ production *ex vivo* following incubation with YAC-1 target tumor cells (Fig. 2D and E). Similarly, NK cells from Cl13-infected mice exhibited greater cytotoxicity against YAC-1 target tumor cells *in vitro* (Fig. 2F), consistent with increased NK cell effector function. These results suggested that chronic virus infection increased NK cell effector function when contacting tumor cells.

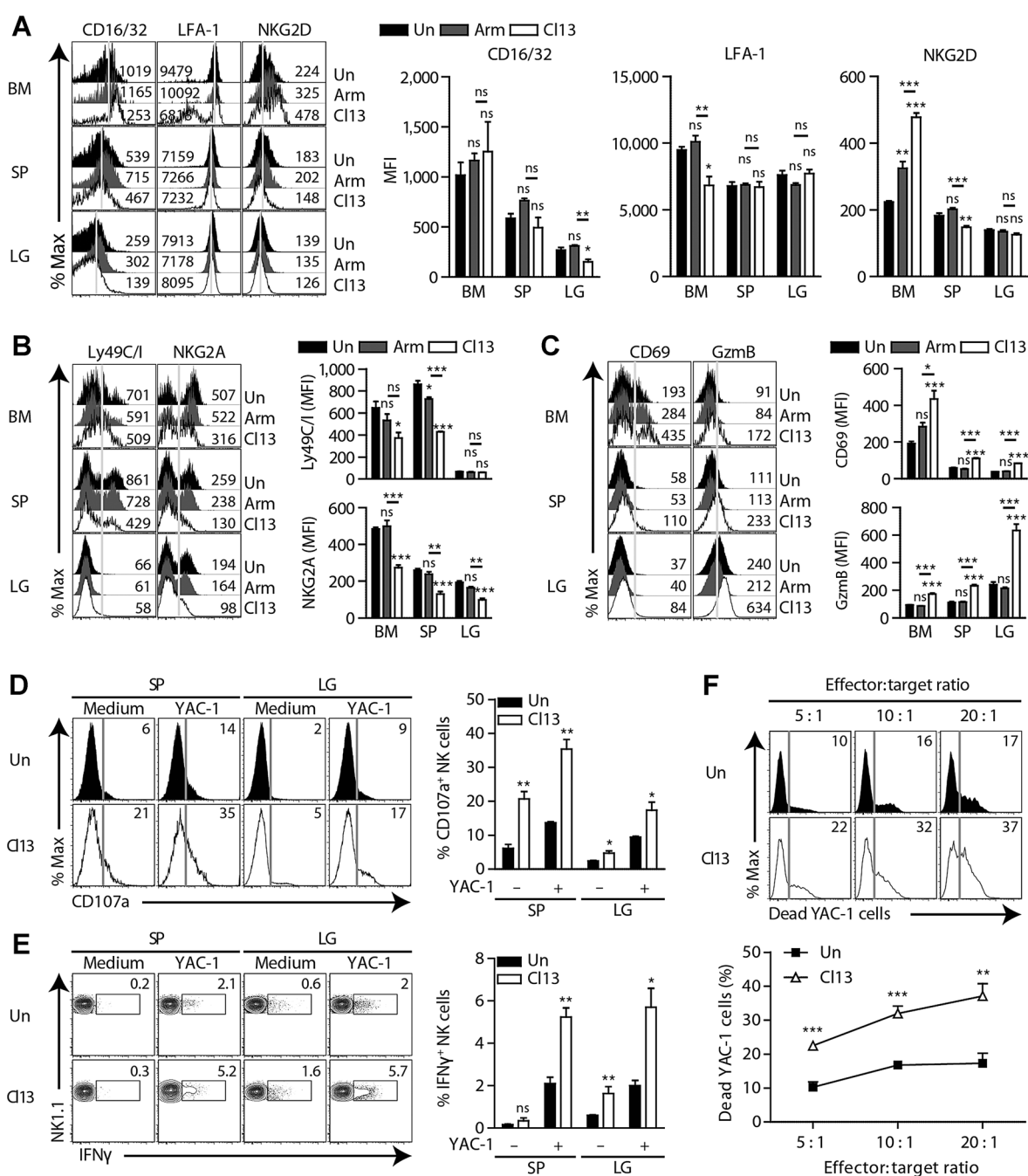
Cl13-infected mice exhibit tumor resistance in an NK cell-dependent manner

NK cells are part of the first line of defense against tumor onset, growth, and metastasis. Therefore, we hypothesized that increased NK cell activation in chronically infected mice would enhance host defenses against tumors. To test this hypothesis, various tumor cells were injected into uninfected mice, Arm-immunized mice (45 dpi), and Cl13-infected mice (45 dpi), and tumor growth and survival rates were monitored. Subcutaneously administered B16F10 melanoma cells, which are sensitive to NK cells due to low MHC class I expression, grew more slowly in Cl13-infected mice compared with the controls (Fig. 3A and B). Similarly, mice intravenously administered B16F10 cells exhibited reduced pulmonary metastases with Cl13 infection, which correlated with increased survival compared with controls (Fig. 3C and D). In a second tumor model, NK cell-resistant cell lines with high MHC class I expression [TC-1 lung adenocarcinoma cells and OVA-expressing EL4 thymoma cells (EG7) cells] were intravenously or subcutaneously injected into each group of mice. Subcutaneous TC-1 and EG7 tumors grew more slowly, elicited fewer lung metastases, and enhanced survival in Cl13-infected mice (Fig. 3E–H; Supplementary Fig. S3A and S3B). These antitumor effects were consistent across several time points up to 100 days after the establishment of chronic infection (Supplementary Fig. S4A–S4C).

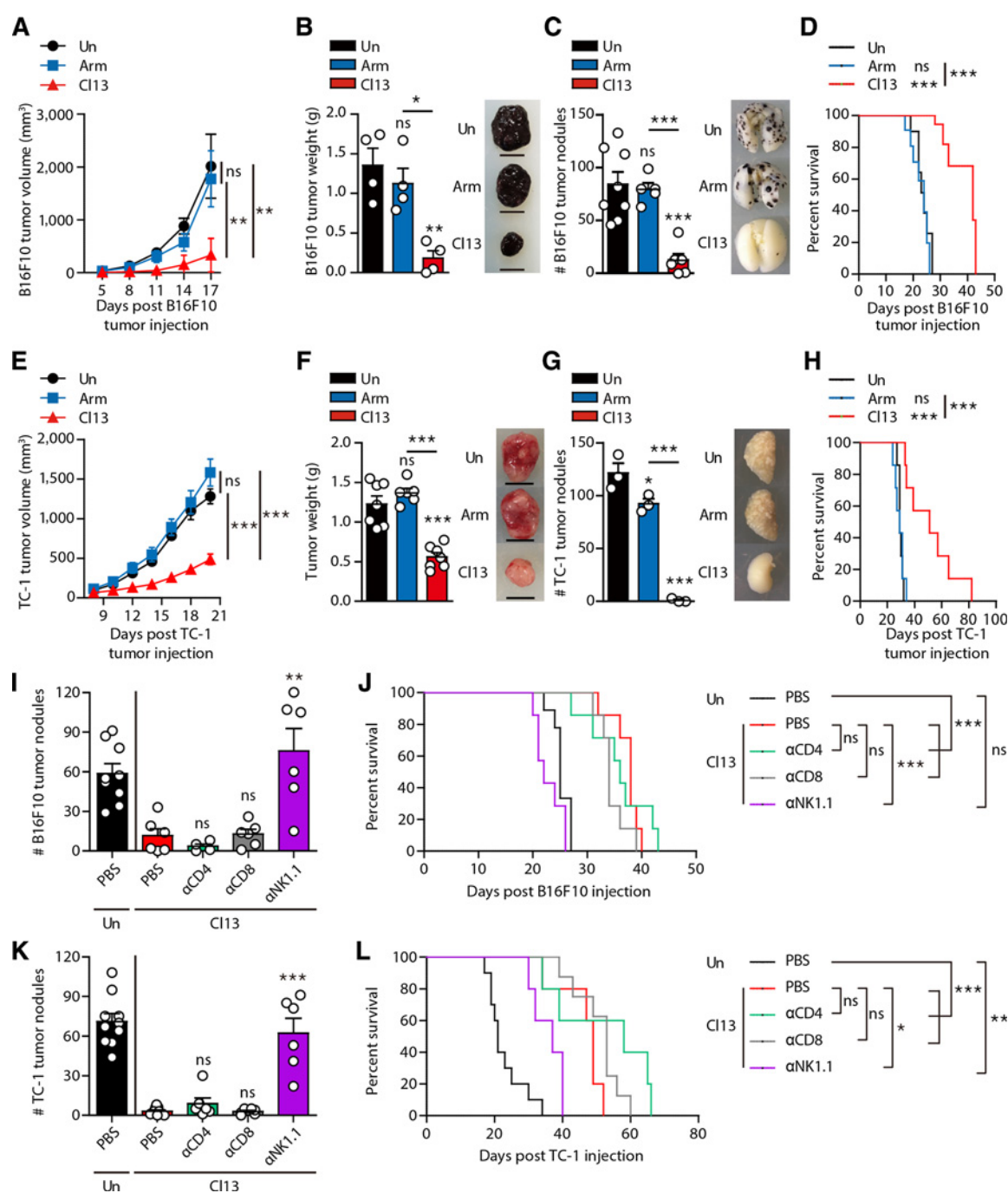
Figure 1.

NK cell phenotypes during late-stage acute and chronic virus infections. **A–F**, C57BL/6 mice were infected with LCMV-Arm or LCMV-Cl13. At 40 dpi, bone marrow (BM), spleen (SP), and lung (LG) NK cells were stained and analyzed by flow cytometry. **A**, Representative flow-cytometric plots and graphs showing the frequencies and absolute numbers of NK cells (NK1.1⁺CD3⁺) in the BM, spleen, and lungs. **B**, Expression patterns of maturation markers on NK cells *ex vivo*. CD27, CD11b, and KLRG1 expression was analyzed in BM, spleen, and lung NK cells. The numbers in the plots indicate the percentage of immature (CD27^{low}CD11b^{low}, CD27^{high}CD11b^{low}, CD27^{high}CD11b^{high}, and CD11b^{high}KLRG1^{low}) and mature (CD27^{low}CD11b^{high} and CD11b^{high}KLRG1^{high}) NK cells. **C**, T-bet expression in NK cells were analyzed by intracellular staining. Representative T-bet expression [mean fluorescence intensity (MFI), left] and summarized (right) results in immature (CD11b⁺KLRG1⁻) and mature (CD11b⁺KLRG1⁺) NK cells are shown. **D**, Representative plot and graph showing the percentages of Ki-67⁺ NK cells. **E**, 7-AAD and Annexin V expression in NK cells *ex vivo*. Representative plot and graph showing the percentages of late-apoptotic NK cells (7AAD⁺ Annexin V⁺). **F**, Splenic NK cells were cultured for 4 days with IL2 (500 U/mL) and then analyzed for 7AAD⁺ and Annexin V⁺ expression. Numbers in the plots indicate the percentages of 7AAD⁺ Annexin V⁻ (necrotic), 7AAD⁺ Annexin V⁺ (late apoptotic), and 7AAD⁻ Annexin V⁺ (early apoptotic) NK cells. Double-negative (DN), Annexin V⁺ (AV⁺), 7AAD⁺, and double-positive (DP) NK cell percentages are also summarized in the graphs. One-way ANOVA with *post hoc* Tukey test was used to test the statistical significance. All bar graphs show mean \pm SEM. Data are representative of at least four independent experiments ($n = 3\text{--}4$ /group in each experiment). *, $P < 0.05$; **, $P < 0.01$; ***, $P < 0.001$. ns, not significant.

Oh et al.

**Figure 2.**

NK cell-mediated cytotoxicity is enhanced in LCMV-CI13-infected mice. **A–C**, C57BL/6 mice were infected with the LCMV-Arm or LCMV-CI13. At 40 dpi, bone marrow, spleen, and lung NK cells were stained and analyzed by flow cytometry. **A**, Activating receptor expression in bone marrow, spleen, and lung NK cells. Numbers in the plots indicate activating receptor MFI. The MFIs of NK receptors in the indicated tissues are also summarized. **B**, Inhibitory receptor (Ly49C/I and NKG2A) expression in bone marrow, spleen, and lung NK cells. Numbers in the plots denote Ly49C/I and NKG2A MFI. The MFI of each NK receptor in the indicated tissues is also summarized. **C**, CD69 and GzmB expression in bone marrow, spleen, and lung NK cells. Numbers in the plots indicate CD69 and GzmB MFI on NK cells. The CD69 and GzmB MFI in NK cells in the indicated tissues are also summarized. **D** and **E**, Lymphocytes isolated from the spleen and lungs of uninfected or CI13-infected mice at 45 dpi were restimulated *in vitro* with YAC-1 cells (E:T ratio: 10:1; 5 hours). **D**, CD107a expression and **E**, IFN γ accumulation were evaluated. Representative plots are shown for expression of CD107a and accumulation of IFN γ in NK cells. Numbers in the plots indicate the percentages of CD107a $^{+}$ or IFN γ $^{+}$ NK cells. The graph summarizes the percentages of CD107a $^{+}$ or IFN γ $^{+}$ NK cells. **F**, *In vitro* cytotoxicity of lung NK cells toward YAC-1 targets (E:T ratio: 5:1, 10:1, and 20:1) quantified by flow cytometric analysis of TO-PRO-3 iodide $^{+}$ YAC-1 cells. Numbers in the plots indicate TO-PRO-3 iodide $^{+}$ YAC-1 cells. The graph summarizes the percentages of TO-PRO-3 iodide $^{+}$ YAC-1 cells. Data were analyzed by one-way ANOVA with (**A–C**) *post hoc* Tukey test and (**D–F**) two-tailed unpaired Student *t* test. All graphs show mean \pm SEM. Data are representative of at least three independent experiments ($n = 3–4$ /group in each experiment). *, $P < 0.05$; **, $P < 0.01$; ***, $P < 0.001$. ns, not significant.

**Figure 3.**

Tumor cells are rejected in LCMV-Cl13-infected mice in an NK cell-dependent manner. **A-D**, B16F10 or (**E-H**) TC-1 tumor cells (5×10^5 cells/mouse) were injected (**A-B**, **E-F**) subcutaneously or (**C-D**, **G-H**) i.v. into uninfected, Arm-immunized (45 dpi), and Cl13-infected mice (45 dpi). **A-B**, **E-F**, Tumor size was monitored every 3 to 4 days, and tumor weight was measured at (**B**) day 17 or (**F**) day 20 after tumor injection. Scale bars, 1 cm. **C** and **G**, 17 days after tumor inoculation, tumor nodules were measured in lungs from each group of mice. **D** and **H**, Survival after B16F10 or TC-1 tumor cell injection (i.v.). **I** and **J**, B16F10 or (**K-L**) TC-1 tumor cells (5×10^5 cells/mouse) were injected i.v. into uninfected and Cl13-infected mice (45 dpi). **I-L**, Depleting anti-CD4, anti-CD8, or anti-NK1.1 or PBS (negative control) was administered i.v. into Cl13-infected mice prior to tumor injection (amounts of each depleting antibody: 1 mg) and at days 5 and 15 (amounts of each depleting antibody: 0.5 mg) after tumor injection. **I**, **K**, After sacrifice, tumor nodules in the lungs at day 17 after tumor inoculation were measured, and (**J**, **L**) survival rates after tumor inoculation were evaluated. Data were analyzed by (**A-C**, **E-G**) one-way ANOVA with *post hoc* Tukey test or (**I**, **K**) Dunnett test. **I**, **K**, Statistical significance was determined by comparison between PBS-treated Cl13-infected mice and anti-CD4-, anti-CD8-, or anti-NK1.1-treated Cl13-infected mice. All line graphs and bar graphs show mean \pm SEM. All survival graphs were analyzed using the Mantel-Cox log-rank test ($n = 5-10$). **A**, **B**, **G**, Data are representative of at least two independent experiments ($n = 3-4$ /group in each experiment). **C-F**, **H-L**, Data are pooled from two experiments ($n = 3-7$ /group in each experiment). *, $P < 0.05$; **, $P < 0.01$; ***, $P < 0.001$. ns, not significant.

In light of the observation that NK cell-resistant tumor growth was inhibited in Cl13-infected mice, we performed TIL analysis in the EG7 tumor model to compare the effector functions of T cells and NK cells. The number of CD4⁺ T, CD8⁺ T, or NK cells in tumors from Cl13-infected mice was similar or decreased compared with uninfected and Arm-immunized groups, respectively (Supplementary Fig. S3C). Cl13-infected mice exhibited 10-fold lower LCMV-specific CD8⁺ T-cell responses than Arm-immunized mice but showed higher tumor-specific CD8⁺ T-cell responses than uninfected or Arm-immunized mice (Supplementary Fig. S3D). NK cells in the tumor from Cl13-infected mice exhibited higher effector functions than the control groups and showed significantly higher IFN γ production than the same group of CD8⁺ T cells. Both CD8⁺ T-cell and NK cell effector functions were inversely correlated with tumor weight, although the effect was much stronger for NK cell effector functions (Supplementary Fig. S3E).

To confirm that this antitumor response was mediated by NK cells, B16F10 or TC-1 tumor cells were injected into Cl13-infected mice (45 dpi) following depletion of CD4⁺ T, CD8⁺ T, or NK cells. Depletion was confirmed in the bone marrow, spleen, and lungs of Cl13-infected mice 17 days after antibody administration (Supplementary Fig. S5A). The viral load in the serum was not altered in Cl13-infected mice with CD4, CD8, or NK1.1 depletion at 10 and 20 days after antibody administration (Supplementary Fig. S5B). Depletion of CD4⁺ or CD8⁺ T cells had no overt effect on the enhanced antitumor responses of Cl13-infected mice. In contrast, the depletion of NK1.1⁺ cells in Cl13-infected mice resulted in increased lung metastases and reduced survival of the mice (Fig. 3I–L). These results indicated that tumor formation was suppressed in Cl13-infected mice in an NK cell-dependent manner.

NK cell cytotoxicity and antitumor immunosurveillance are related to viral load

To investigate the influence of viral load on antitumor immunity in chronically infected mice, we used a conventional Cl13 infection model without CD4⁺ T-cell depletion prior to infection. In this model, the viral load gradually decreases, and after 60 days, most of the virus disappears from organs except the brain and kidney. The relationship between the viral titer and the frequency of Gzmb⁺ NK cells was similar in the spleens of Arm-infected, Cl13-infected, and CD4⁺ T-cell-depleted/Cl13-infected groups (Fig. 4A and B). On day 32, the mice infected with Cl13 (without CD4⁺ T-cell depletion) had lower (and more variable) viral titers in the sera compared with mice infected with Cl13 after depletion of CD4⁺ T cells (Fig. 4C). The expression levels of Gzmb and CD69 in peripheral NK cells of mice infected with Cl13 (without CD4⁺ T-cell depletion) were higher than those of uninfected mice but were lower than those of Cl13-infected mice after depletion of CD4⁺ T cells (Fig. 4D). Furthermore, viral titers and expression of Gzmb and CD69 were correlated with the peripheral blood NK cells from mice infected with Cl13 (without CD4⁺ T-cell depletion; Fig. 4E). These results suggested that the NK cell cytotoxicity was linked to virus titer.

To determine whether antitumor immunity is associated with the severity of chronic viral infection, tumor progression was analyzed following i.v. injection of TC-1 tumor cells in two different Cl13 infection models. A significant reduction in the antitumor effect in mice infected with Cl13 (without CD4⁺ T-cell

depletion) was seen compared with mice infected with Cl13 after depletion of CD4⁺ T cells (Fig. 4F–H). The inhibition of tumor progression was not due to direct LCMV infection of the tumor cells because tumor cell infection with LCMV did not inhibit their proliferation *in vitro* (Supplementary Fig. S6A). Replication of LCMV in the tumor microenvironment was like that in other organs (Supplementary Fig. S6B). These results indicated that LCMV did not directly inhibit tumor progression in LCMV-infected mice and that high viral titers increased NK cell cytotoxicity, thereby maintaining immune surveillance.

Chronic inflammatory niches contribute to enhanced NK cell cytotoxicity

To determine how the inflammatory environment leads to enhanced NK cell cytotoxicity, splenocytes (Ly5.1/5.1) isolated from uninfected mice were injected into the peritoneal cavity of uninfected mice (Ly5.2/5.2) or Cl13-infected mice (Ly5.2/5.2, 46 dpi). After 72 hours, adoptively transferred donor NK cells from recipients were analyzed for Gzmb protein expression (Fig. 5A). The donor NK cells recovered from Cl13-infected recipients displayed increased Gzmb expression compared with those from uninfected recipients (Fig. 5B). These findings confirmed that Gzmb in NK cells increased upon exposure to the environment generated by chronic LCMV infection.

Various cytokines regulate NK cell development, homeostasis, and function during viral infection (26). To identify cytokines involved in regulating NK cell phenotype and function during chronic virus infection, cytokines were measured in the sera of Cl13-infected mice (41 dpi). Several cytokines known to be involved in NK cell activation were elevated in Cl13-infected mice, including IL2, IL12, IL15, IL21, and IFN β (Fig. 5C). These data suggested that the inflammatory environment elicited by chronic LCMV infection enhanced NK cell cytotoxicity.

Chronic LCMV infection modulates responsiveness to type I IFNs via increased STAT1

To determine which cytokines had the greatest effect on NK cells, splenic NK cells from uninfected, Arm-immunized, and Cl13-infected mice were analyzed for various STAT mRNAs by qRT-PCR. Only STAT1 mRNA was significantly higher in NK cells from Cl13-infected mice compared with uninfected or Arm-immunized mice (Fig. 6A). STAT1 protein expression was also significantly higher in NK and T cells from Cl13-infected mice compared with uninfected or Arm-immunized mice (Fig. 6B). Previous studies showed that NK cells have high basal expression of STAT4, but that STAT1 predominates via continuous exposure to type I IFNs during acute LCMV or chronic HCV infection (27, 28), and type I IFNs increase the cytotoxicity of NK cells via the STAT1–Gzmb axis during flu infection (29). Based on these reports, it is likely that type I IFNs predominantly contribute to enhanced NK cell cytotoxicity during chronic viral infection.

To analyze type I IFN-mediated activation of STAT1 and STAT4 in NK cells from uninfected, Arm-immunized, and Cl13-infected mice, NK cells were incubated without cytokine stimulation to allow them to return to basal states, followed by stimulation with IFN β , IFN γ , and IL12. IFN γ and IL12 phosphorylate STAT1 and STAT4, respectively, whereas IFN β phosphorylates both STAT1 and STAT4 in NK cells. Consistent with previous studies in acute LCMV and chronic HCV infection models, NK cells from Cl13-infected mice exhibited higher

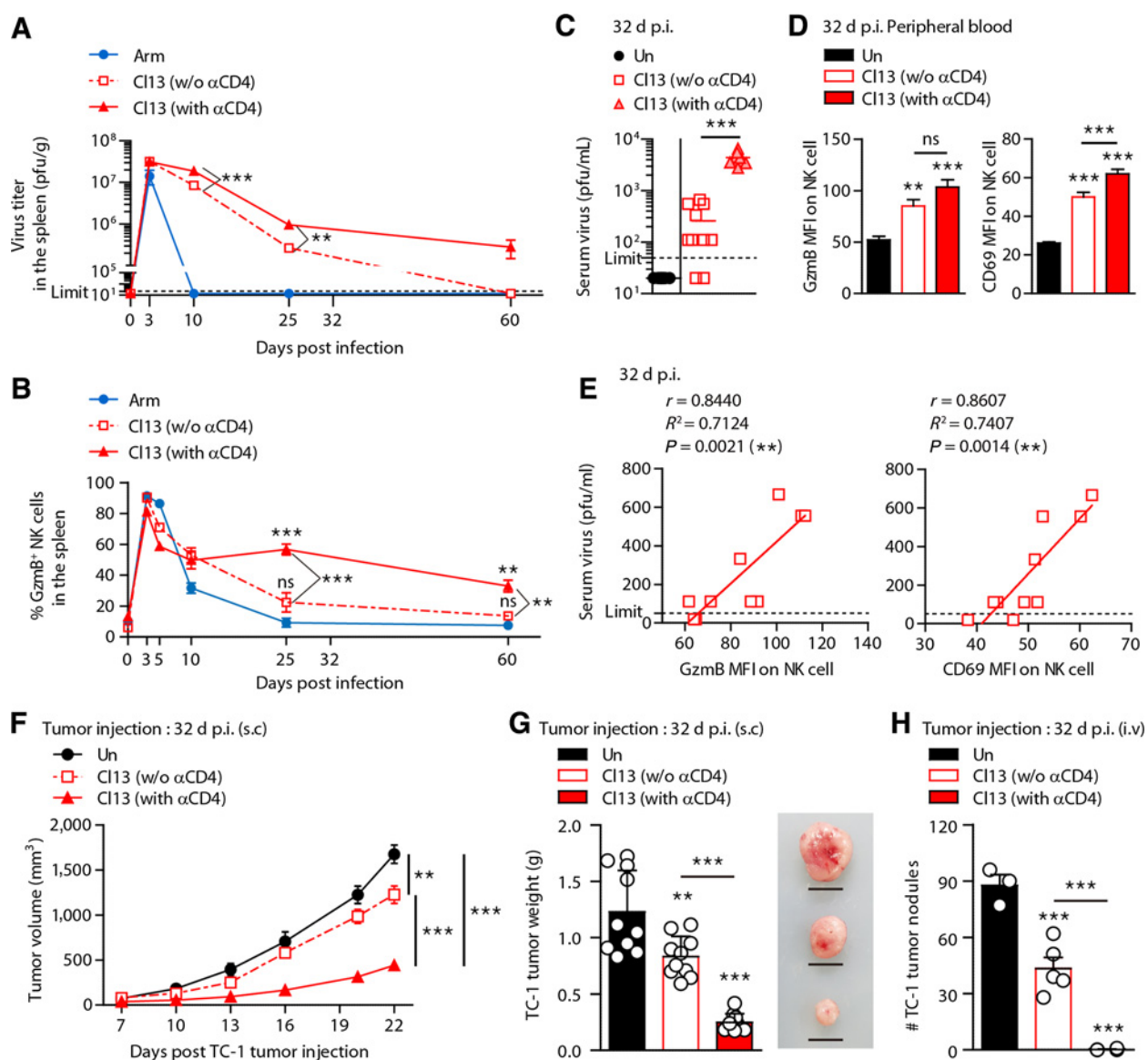


Figure 4.

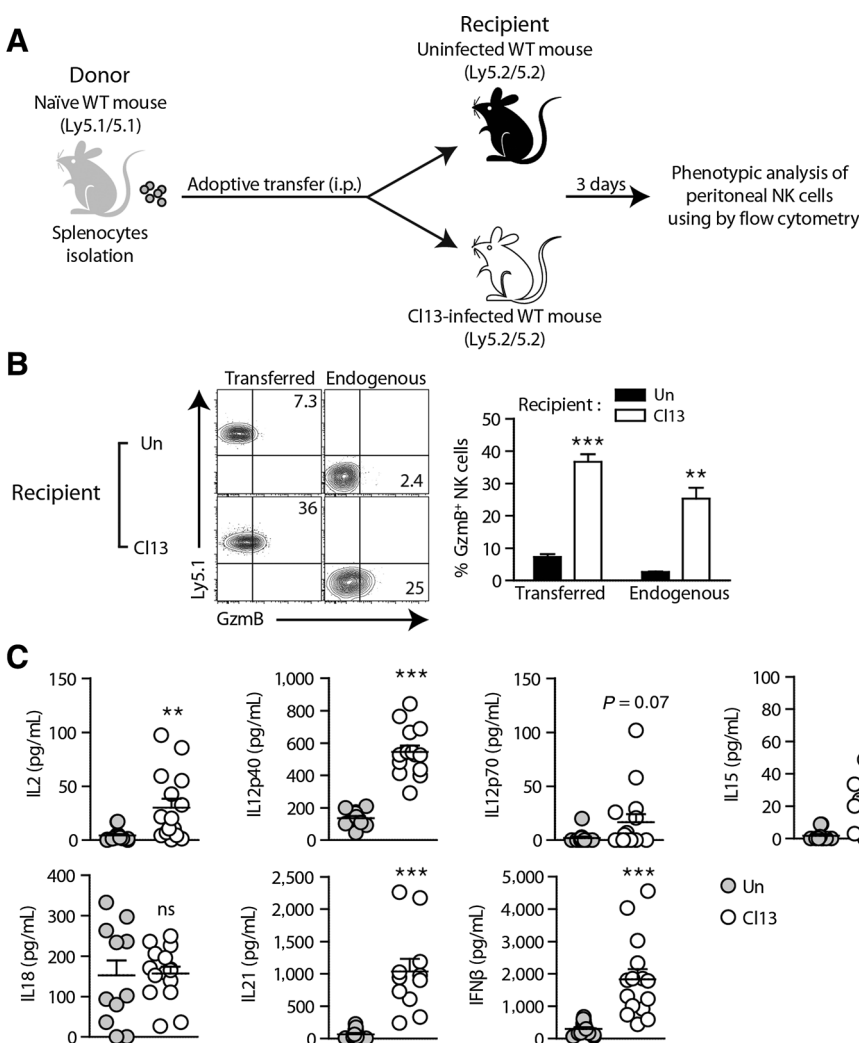
NK cell-mediated immunosurveillance is associated with the severity of chronic viral infection. Mice were infected with LCMV-Arm, LCMV-CI13 (without anti-CD4), or LCMV-CI13 after depletion of CD4⁺ T cells (with anti-CD4: 0.2 mg on days -1 and 0 relative to infection with LCMV-CI13 on day 0). **A**, Kinetics of viral titer in the spleen during acute and chronic viral infection at the indicated time post-infection. Dashed black line: the virus detection limit. **B**, Kinetics of Gzmb⁺ NK cells during acute and chronic viral infection. Representative graph showing Gzmb⁺ NK cell percentages in spleens at the indicated time after infection. **C-E**, On day 32 after virus infection, viral titer in the (C) sera, (D) Gzmb, and CD69 MFI in NK cells in the peripheral blood and (E) their correlation was analyzed. **F-H**, TC-1 tumor cells (5×10^5 cells/mouse) were injected (F, G) subcutaneously or (H) i.v. into each group of mice at 32 dpi, tumor size was monitored every 2 to 4 days, and tumor weight and nodules were measured at day 22 after tumor injection. Scale bars, 1 cm. **A, C**, Data were analyzed by two-tailed unpaired Student *t* test, (**B, D, F-H**) one-way ANOVA with *post hoc* Tukey test, and (E) Pearson correlation. All line graphs and bar graphs show mean \pm SEM. **A, B**, Data are pooled from three experiments ($n = 3$ /group in each experiment). **C-H**, Data are representative of at least two independent experiments ($n = 3-10$ /group in each experiment). **, $P < 0.01$; ***, $P < 0.001$. ns, not significant.

phosphorylated (p)STAT1 in response to IFN β or IFN γ but lower pSTAT4 in response to IFN β or IL12 compared with those from uninfected or Arm-immunized mice (Fig. 6C and D). Overall, these results suggested that IFN-mediated STAT1/4 activation in response to type I IFNs in NK cells from CI13-infected mice shifted toward activation of pSTAT1 rather than pSTAT4 due to an increase in STAT1 expression.

Type I IFNs directly activate NK cells during chronic LCMV infection

To determine whether the increased cytotoxicity of NK cells is dependent upon type I IFN signaling, we performed *in vivo* blockade experiments using anti-IFN- α/β receptor 1 (anti-IFNAR1), which efficiently blocks type I IFN signaling. At day 5 after antibody treatment, the spleen and lung lymphocytes of

Oh et al.

**Figure 5.**

NK cells from naïve mice acquire cytotoxic phenotypes after transfer to LCMV-CI13-infected mice. **A** and **B**, Splenocytes from naïve mice (Ly5.1/5.1) were transferred i.p. into uninfected mice (Ly5.2/5.2) or CI13-infected mice (Ly5.2/5.2, 46 dpi), respectively. At 3 days after transfer, peritoneal cells were analyzed for NK cell Gzmb expression. Representative plots show the percentages of Gzmb⁺ NK cells in uninfected or CI13-infected recipients. **C**, Serum cytokines in uninfected mice or CI13-infected mice (41 dpi). Two-tailed unpaired Student *t* test was used to test the statistical significance. All graphs show mean ± SEM. Data are representative of at least two independent experiments (*n* = 4–15/group in each experiment). **, *P* < 0.01; ***, *P* < 0.001. ns, not significant.

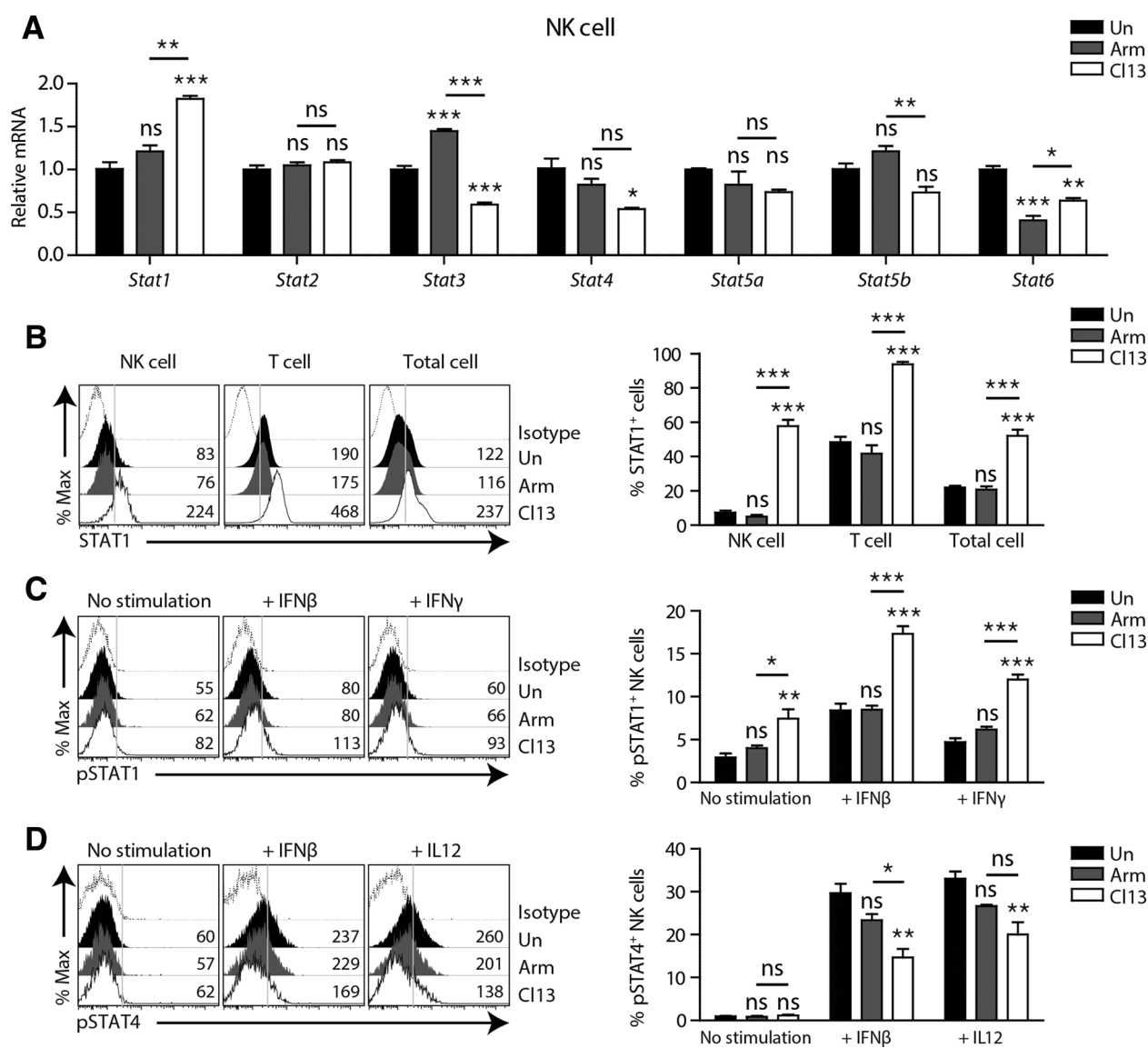
CI13-infected mice were analyzed (Fig. 7A). Type I IFN signaling blockade significantly reduced STAT1, CD69, and Gzmb expression in NK cells from CI13-infected mice (Fig. 7B and C), and IFNAR1 blockade diminished the NK cell effector functions induced by coculture with tumor cells (Fig. 7D). Collectively, these data indicated that the enhancement of NK cell cytotoxicity in chronically infected mice required type I IFN receptor signaling.

To identify whether type I IFNs directly activate NK cells in CI13-infected mice, we injected splenocytes (WT: Ly5.1/Ly5.2 and IFNAR1^{-/-}: Ly5.2/5.2) from uninfected mice into WT-uninfected or WT-CI13-infected mice (Ly5.1/5.1, 45 dpi). After 72 hours, the mice were sacrificed, and endogenous and adoptively transferred NK cells were analyzed (Fig. 7E). As expected, adoptively transferred WT NK cells from CI13-infected recipients expressed high STAT1 and Gzmb compared with NK cells from uninfected recipients. In contrast to WT NK cells, IFNAR1^{-/-} NK cells did not upregulate the expression of cytotoxic molecules in CI13-infected recipients compared with those from uninfected recipients (Fig. 7F). This is consistent with a role for type I IFNs in directly activating NK cells during chronic LCMV infection.

To assess whether type I IFN signaling is critical for the NK cell-mediated antitumor responses in CI13-infected mice, we injected anti-IFNAR1, anti-NK1.1, or a combination of both into CI13-infected mice (40 dpi) 1 day prior to TC-1 tumor injection and at 5 and 15 days after tumor injection. Twenty-one days after tumor injection, IFNAR1 blockade resulted in 20% increased tumor metastasis in CI13-infected mice, suggesting that type I IFN signaling was critical for antitumor immunity (Fig. 7G). However, no additional increase in tumor nodules in the group treated with the combination of antibodies was observed compared with the group treated with anti-NK1.1 alone (Fig. 7G). Collectively, these results indicated that NK cells were indispensable for antitumor immunity via type I IFN signaling in CI13-infected mice.

Discussion

This study demonstrated that the inflammatory milieu generated by a chronic virus infection can enhance NK cell function and inhibit tumor progression. This effect was mediated by type I IFN signaling, which directly augmented NK cell cytotoxicity. These findings indicated that type I IFNs can simultaneously minimize

**Figure 6.**

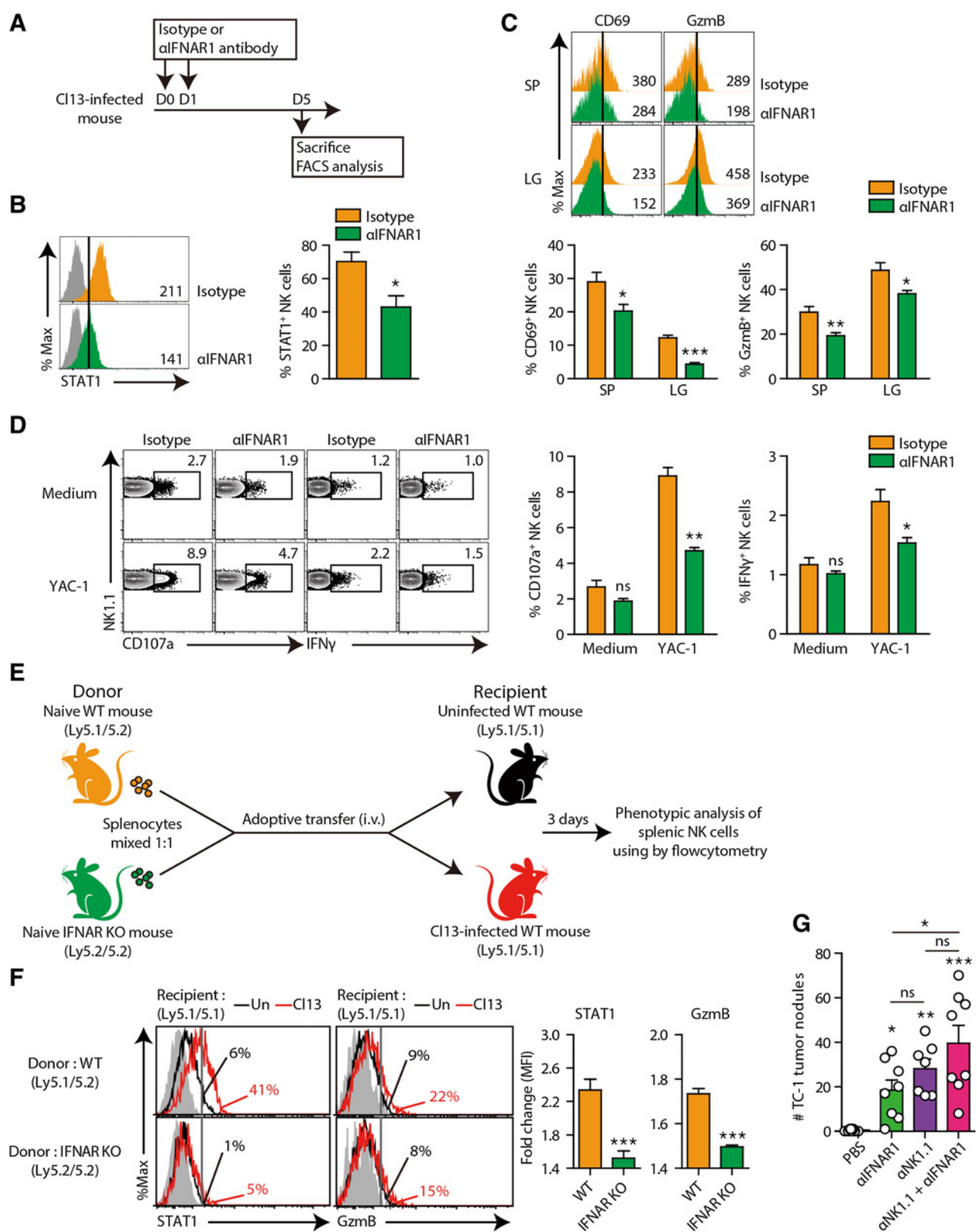
NK cells display increased STAT1 expression and prefer STAT1 over STAT4 phosphorylation in response to $\text{INF}\beta$ during chronic LCMV infection. **A**, mRNA was isolated from splenic NK cells from uninfected, Arm-immune (57 dpi), or CI13-infected mice (57 dpi). mRNA of various STATs were measured by qRT-PCR, normalized to GAPDH, and compared with mRNA in NK cells from uninfected mice to calculate fold induction. **B**, *Ex vivo* STAT1 expression in NK, T, and total cells in the spleen from uninfected, Arm-immune (45 dpi) or CI13-infected mice (45 dpi). Numbers in the plots indicate MFI values. STAT1⁺ cell percentages are summarized. **C** and **D**, Phosphorylation of STAT1 and STAT4 during the NK cell response to $\text{INF}\beta$ (50,000 U/mL) and $\text{INF}\gamma$ (100 ng/mL) or IL12 (200 ng/mL) in the splenic NK cells from uninfected, Arm-immune (45 dpi), or CI13-infected mice (45 dpi). pSTAT1⁺ and pSTAT4⁺ NK cell percentages are summarized. One-way ANOVA with *post hoc* Tukey test was used to test the statistical significance. All bar graphs show mean \pm SEM. **A**, qRT-PCR was performed using mRNA pooled from 30 mice/group. **B–D**, Data are representative of at least two independent experiments ($n = 3\text{--}4/\text{group}$ in each experiment). *, $P < 0.05$; **, $P < 0.01$; ***, $P < 0.001$. ns, not significant.

T-cell-mediated pathologic damage from an infection and contribute to sustained, or even enhanced, host immune surveillance by upregulating NK cell activity.

Type I IFNs are secreted during the early phases of chronic infections and play an important role in regulating immune responses. Although levels decline in the later phases of chronic infection due to numerous negative regulators (30), studies have shown that residual type I IFNs play an important role in preventing excessive T-cell activation LCMV mouse models (10, 11).

For HCV, persistent interferon-stimulated gene expression is observed during chronic infection (31). In HCV-infected patients, sustained type I IFN signaling induces increased expression of STAT1 in NK cells, leading to enhanced cytotoxicity and decreased $\text{INF}\gamma$ production (32). The $\text{INF}\gamma$ acts to limit virus spread, whereas the cytolytic activity may act to eliminate virus-specific T cells and prevent T-cell-mediated immunopathology (33). Thus, NK cells may play a critical role in immune regulation by suppressing T-cell responses (16). It is believed that NK cells retain their regulatory

Oh et al.



functions during later stages of a chronic infection by killing virus-specific T cells because depletion of NK cells at later stages of chronic infection results in increased virus-specific T cells and lower virus titers (17). Therefore, Waggoner and colleagues proposed a strategy to restore the T-cell functions and antiviral capacity of chronically infected individuals by removing NK cells (17). However, our study suggested that chronically infected individuals may be susceptible to cancer progression if they do not have NK cells. This paradoxical phenomenon can be viewed as a mechanism of immunologic compensation to protect chronically infected individuals from opportunistic infections or carcinogenesis. We believe that this paradox is resolved by our results showing that NK cells are not exhausted, but rather activated, as the virus titer increases, even though antigen-specific T cells are progressively exhausted during chronic virus infection (23). In this regard, our results indicated that NK cells, but not antigen-specific T cells, provide cancer immunosurveillance during chronic LCMV infection. These beneficial effects on cancer immune surveillance by NK cells during persistent viral infections have also been reported in previous studies (7, 8). Here, we have extended these studies to reveal insights into the mechanism of NK cell-mediated antitumor effects.

Several studies have reported antitumor phenomena in chronically infected patients. First, HCV has been reported to interfere with liver metastasis in colorectal cancer patients. Approximately 35% to 40% of patients with advanced colorectal cancer develop liver metastasis, and although the frequency metastases to the lung was reported to be similar between chronically HCV-infected and uninfected patients, metastases to the liver, the main reservoir of viral replication, decreased by more than 2-fold (34, 35). It was speculated that activated hepatic CD8⁺ T cells might kill nonantigen-bearing bystander cancer cells, but considering our findings, NK cells are more likely to be the key players in patients infected with HCV. Second, reactivation of latent viruses, such as human cytomegalovirus (HCMV), is frequently observed when leukemia patients receive hematopoietic stem cell transplantation, and HCMV reactivation has been correlated with an increase in NK cell maturation (36) and decreased leukemia relapse (37). It is possible that the activation of NK cells due to HCMV recurrence contributes to a reduction in leukemia relapse. Third, chronic HCV infection causes progressive liver fibrosis, which can lead to cirrhosis and hepatocellular carcinoma (HCC). Eradication of the virus can prevent the onset of HCC. Although direct-acting antivirals (DAA) dramatically reduce HCV levels in infected patients (38), studies have demonstrat-

ed a rapid increase in HCC recurrence in HCV patients who received an IFN-free DAA therapy (39, 40). These findings are controversial, but are a clinical concern (41–43). Disruptions in immune surveillance after DAA therapy, such as reduced type I IFN production (44) and NK cell activity (42, 45, 46), have been speculated to cause rapid HCC recurrence. Taken together, our results point to a potential mechanism tying together these various clinical observations.

Anticancer therapy using the immune system has undergone a renaissance, and several therapies, such as virotherapy, immune-checkpoint blockade (ICB), and adoptive cell transfer, have all shown great promise. The mechanism of virotherapy is not yet fully understood, but it can be broadly divided into the recruitment and activation of immune cells by inflammatory cytokines and the direct lysis of tumor cells. According to a published study (47), nononcolytic LCMV showed superior anticancer effects compared with the oncolytic vesicular stomatitis virus widely used in virotherapy. Kalkavan and colleagues found that locally or systemically administered LCMV preferentially replicated in cancer cells, causing Ly6C⁺ monocytes to secrete type I IFNs, resulting in the activation of tumor-specific CD8⁺ T cells and tumor regression (47). In contrast, we did not observe the rapid replication of LCMV. The difference in the two studies may be due to the duration of the viral infection. Here, the tumor cells were injected at the late stage of infection when virus was not actively replicating. Kalkavan and colleagues also acknowledged that T cells were largely dispensable in the mechanisms of antitumor effects of LCMV in the *Tcrab^{-/-}*, *Rag1^{-/-}*, and NOD/SCID mouse models (47). They also found that type I IFNs act directly on tumor regression by reducing angiogenesis rather than activating host cells (47).

ICB is currently receiving a great deal of attention, but many patients do not respond to the therapy. Chronic exposure to IFNs promotes resistance to ICB by upregulating the expression of multiple T-cell inhibitory receptors in tumor cells (48). Consequently, ICB monotherapy may be rendered ineffective in patients with chronic viral infections, and combination therapy with several types of immune-checkpoint inhibitors or NK cell-based therapies may be preferable. Although adoptive T-cell transfer has also been regarded as promising, NK cell-based therapy has not received much attention due to poor clinical outcomes. Most studies have used cytokines, such as IL2 and IL15, to expand and activate NK cells (49). Based on our experimental results, type I IFNs appear to be more suitable for increasing the antitumor activity of NK cells. Direct injection of

Figure 7.

Type I IFN signaling is critical for NK cell cytotoxicity in LCMV-Cl13-infected mice. **A**, Anti-IFNAR1 (0.5 mg) or control isotype antibody (0.5 mg) was administered intravenously (i.v.) twice into Cl13-infected mice at 40 dpi. At 5 days post blockade, splenic and pulmonary NK cells were analyzed. **B**, *Ex vivo* STAT1 expression in splenic NK cells. Numbers in the plots indicate MFI values in NK cells. STAT1⁺ NK cell percentages are summarized. **C**, CD69 and GzmB expression on splenic and pulmonary NK cells. Numbers in the plots indicate the MFI values in NK cells. Percentages of indicated marker-positive NK cells are also depicted in graphs. **D**, Pulmonary NK cells restimulated *in vitro* with YAC-1 cells (E:T ratio: 10:1) were evaluated for CD107a expression and IFN γ accumulation. Representative plot and graphs show the percentages of CD107a⁺ or IFN- γ ⁺ NK cells. **E**, WT (Ly5.1/5.2) or IFNAR1 KO (Ly5.2/5.2) splenocytes were obtained from naïve mice and adoptively transferred i.v. into uninfected or Cl13-infected mice (Ly5.1/5.1, 45 dpi), respectively. At 3 days post transfer, splenocytes were analyzed for STAT1 and GzmB expression in NK cells. **F**, STAT1 and GzmB expression in NK cells from uninfected or Cl13-infected recipients. Graphs represent the fold increase in expression (MFI) of donor cells from WT or IFNAR1 KO splenocytes in Cl13-infected recipients compared with uninfected recipients. **G**, Anti-IFNAR1 (day -4: 1 mg; days 5 and 15: 0.5 mg), anti-NK1.1 (day -4: 1 mg; days 5 and 15: 0.5 mg), or combination of both (day -4 anti-IFNAR1 and anti-NK1.1: 1 mg; days 5 and 15 anti-IFNAR1 and anti-NK1.1: 0.5 mg) was administered i.v. into Cl13-infected mice (40 dpi). At day 21 post tumor injection (5×10^5 cells/mouse; i.v.), mice were sacrificed, and tumor nodules in the lungs were measured. **B–F**, Data were analyzed by two-tailed unpaired Student t test and (**G**) one-way ANOVA with *post hoc* Dunnett test. All bar graphs show the mean \pm SEM. **B, D**, Data are representative of at least two independent experiments ($n = 3–4$ /group in each experiment). **C, F, G**, Data are pooled from two experiments ($n = 3–4$ /group in each experiment). *, $P < 0.05$; **, $P < 0.01$; ***, $P < 0.001$. ns, not significant.

type I IFNs induces antitumor responses by multiple mechanisms, including stimulation of innate and adaptive immune cells and direct inhibition of tumor growth. However, considerable challenges remain, such as reducing tissue toxicity and increasing the half-life of the cytokine *in vivo*. Indeed, from the late 1970s to the mid-1980s, there were many attempts to use type I IFNs as tools in anticancer treatment, but it is not widely used now. Various strategies are being attempted to directly deliver type I IFNs to the tumor microenvironment to overcome these limitations (50). These approaches might constitute a safe and potent antitumor therapy when combined with NK cell transfer therapy.

Taken together, our findings revealed that chronic viral infections and type I IFNs drive NK cells into a terminally differentiated phenotype characterized by higher cytotoxicity and reduced inhibitory receptor expression. These activated NK cells can play key roles in general antitumor immune surveillance, and these findings redefine our understanding for the role of immunosuppression of type I IFNs and NK cells in chronic viral infections. These data could help facilitate the development of more effective treatment strategies for a variety of cancer patients.

Disclosure of Potential Conflicts of Interest

No potential conflicts of interest were disclosed.

References

- Wherry EJ. T cell exhaustion. *Nat Immunol* 2011;12:492–9.
- Stelekati E, Wherry EJ. Chronic bystander infections and immunity to unrelated antigens. *Cell Host Microbe* 2012;12:458–69.
- Tillmann HL, Heiken H, Knapik-Botor A, Heringlake S, Ockenga J, Wilber JC, et al. Infection with GB virus C and reduced mortality among HIV-infected patients. *N Engl J Med* 2001;345:715–24.
- Xiang J, Wunschmann S, Diekema DJ, Klinzman D, Patrick KD, George SL, et al. Effect of coinfection with GB virus C on survival among patients with HIV infection. *N Engl J Med* 2001;345:707–14.
- Barton ES, White DW, Cathelyn JS, Brett-McClellan KA, Engle M, Diamond MS, et al. Herpesvirus latency confers symbiotic protection from bacterial infection. *Nature* 2007;447:326–9.
- Ingram JT, Yi JS, Zajac AJ. Exhausted CD8 T cells downregulate the IL-18 receptor and become unresponsive to inflammatory cytokines and bacterial co-infections. *PLoS Pathog* 2011;7:e1002273.
- Bukowski JF, Biron CA, Welsh RM. Elevated natural killer cell-mediated cytotoxicity, plasma interferon, and tumor cell rejection in mice persistently infected with lymphocytic choriomeningitis virus. *J Immunol* 1983;131:991.
- White DW, Keppel CR, Schneider SE, Reese TA, Coder J, Payton JE, et al. Latent herpesvirus infection arms NK cells. *Blood* 2010;115:4377–83.
- Odorizzi PM, Wherry EJ. An interferon paradox. *Science* 2013;340:155–6.
- Wilson EB, Yamada DH, Elsaesser H, Herskovitz J, Deng J, Cheng G, et al. Blockade of chronic type I interferon signaling to control persistent LCMV infection. *Science* 2013;340:202–7.
- Teijaro JR, Ng C, Lee AM, Sullivan BM, Sheehan KCF, Welch M, et al. Persistent LCMV infection is controlled by blockade of type I interferon signaling. *Science* 2013;340:207–11.
- Taleb K, Auffray C, Villefroy P, Pereira A, Hosmalin A, Gaudry M, et al. Chronic type I IFN is sufficient to promote immunosuppression through accumulation of myeloid-derived suppressor cells. *J Immunol* 2017;198:1156–63.
- Welsh JR. Cytotoxic cells induced during lymphocytic choriomeningitis virus infection of mice. I. Characterization of natural killer cell induction. *J Exp Med* 1978;148:163–81.
- Crome SQ, Lang PA, Lang KS, Ohashi PS. Natural killer cells regulate diverse T cell responses. *Trends Immunol* 2013;34:342–9.
- Lang PA, Lang KS, Xu HC, Grusdat M, Parish IA, Recher M, et al. Natural killer cell activation enhances immune pathology and promotes chronic infection by limiting CD8+ T-cell immunity. *Proc Natl Acad Sci USA* 2012;109:1210–5.
- Waggoner SN, Cornberg M, Selin LK, Welsh RM. Natural killer cells act as rheostats modulating antiviral T cells. *Nature* 2011;481:394–8.
- Waggoner SN, Daniels KA, Welsh RM. Therapeutic depletion of natural killer cells controls persistent infection. *J Virol* 2014;88:1953–60.
- Ahmed R, Salmi A, Butler LD, Chiller JM, Oldstone MB. Selection of genetic variants of lymphocytic choriomeningitis virus in spleens of persistently infected mice. Role in suppression of cytotoxic T lymphocyte response and viral persistence. *J Exp Med* 1984;160:521.
- Wherry EJ, Blattman JN, Murali-Krishna K, Van Der Most R, Ahmed R. Viral persistence alters CD8 T-cell immunodominance and tissue distribution and results in distinct stages of functional impairment. *J Virol* 2003;77:4911–27.
- Miyagi T, Lee S-H, Biron CA. Intracellular staining for analysis of the expression and phosphorylation of signal transducers and activators of transcription (STATs) in NK cells. *Methods Mol Biol*. 2010:159–75.
- Lee-MacAry AE, Ross EL, Davies D, Laylor R, Honeychurch J, Glennie MJ, et al. Development of a novel flow cytometric cell-mediated cytotoxicity assay using the fluorophores PKH-26 and TO-PRO-3 iodide. *J Immunol Methods* 2001;252:83–92.
- Nociari M, Ocheretina O, Murphy M, Falck-Pedersen E. Adenovirus induction of IRF3 occurs through a binary trigger targeting Jun N-terminal kinase and TBK1 kinase cascades and type I interferon autocrine signaling. *J Virol* 2009;83:4081–91.
- Blackburn SD, Shin H, Haining WN, Zou T, Workman CJ, Polley A, et al. Coregulation of CD8+ T cell exhaustion by multiple inhibitory receptors during chronic viral infection. *Nat Immunol* 2009;10:29–37.
- Huntington ND, Voshchenrich CAJ, Di Santo JP. Developmental pathways that generate natural-killer-cell diversity in mice and humans. *Nat Rev Immunol* 2007;7:703–14.
- Vivier E, Tomasello E, Baratin M, Walzer T, Ugolini S. Functions of natural killer cells. *Nat Immunol* 2008;9:503–10.

Authors' Contributions

Conception and design: J.H. Oh, Y.H. Ban, K.-M. Lee, S.-J. Ha
Development of methodology: J.H. Oh, Y.H. Ban
Acquisition of data (provided animals, acquired and managed patients, provided facilities, etc.): J.H. Oh, M.J. Kim, Y.H. Ban, H.K. Lee, S.-J. Ha
Analysis and interpretation of data (e.g., statistical analysis, biostatistics, computational analysis): J.H. Oh, M.J. Kim, Y.H. Ban, K.-M. Lee, S.-J. Ha
Writing, review, and/or revision of the manuscript: J.H. Oh, M.J. Kim, E.-C. Shin, S.-J. Ha
Administrative, technical, or material support (i.e., reporting or organizing data, constructing databases): J.H. Oh, M.J. Kim, S.J. Choi, Y.H. Ban, S.-J. Ha
Study supervision: E.-C. Shin, S.-J. Ha

Acknowledgments

This study was supported by the Basic Science Research Program (2018R1A2A1A05076997 and 2017R1A5A1014560 to S.-J. Ha and 2017R1A2B3004828 to K.-M. Lee) and the Bio & Medical Technology Development Program (2018M3A9H3024850 to S.-J. Ha) through the National Research Foundation of Korea (NRF) funded by the Ministry of Science, ICT & Future Planning.

The costs of publication of this article were defrayed in part by the payment of page charges. This article must therefore be hereby marked *advertisement* in accordance with 18 U.S.C. Section 1734 solely to indicate this fact.

Received June 18, 2018; revised December 3, 2018; accepted February 21, 2019; published first February 26, 2019.

26. Marçais A, Viel S, Grau M, Henry T, Marvel J, Walzer T. Regulation of mouse NK cell development and function by cytokines. *Front Immunol* 2013;4:450.
27. Miyagi T, Gil MP, Wang X, Louten J, Chu WM, Biron CA. High basal STAT4 balanced by STAT1 induction to control type 1 interferon effects in natural killer cells. *J Exp Med* 2007;204:2383–96.
28. Miyagi T, Takehara T, Nishio K, Shimizu S, Kohga K, Li W, et al. Altered interferon-alpha-signaling in natural killer cells from patients with chronic hepatitis C virus infection. *J Hepatol* 2010;53:424–30.
29. Guan J, Miah SM, Wilson ZS, Erick TK, Banh C, Brossay L. Role of type I interferon receptor signaling on NK cell development and functions. *PLoS One* 2014;9:e111302.
30. Porritt RA, Hertzog PJ. Dynamic control of type I IFN signalling by an integrated network of negative regulators. *Trends Immunol* 2015;36:150–60.
31. Su AI, Pezacki JP, Wodicka L, Brideau AD, Supekova L, Thimme R, et al. Genomic analysis of the host response to hepatitis C virus infection. *PNAS* 2002;99:15669–74.
32. Rehmann B. Pathogenesis of chronic viral hepatitis: Differential roles of T cells and NK cells. *Nat Med* 2013;19:859–68.
33. Guidotti LG, Chisari FV. To kill or to cure: options in host defense against viral infection. *Curr Opin Immunol* 1996;8:478–83.
34. Destri GL, Castaing M, Ferlito F, Minutolo V, Di Cataldo A, Puleo S. Rare hepatic metastases of colorectal cancer in livers with symptomatic HBV and HCV hepatitis. *Ann Ital Chir* 2013;84:323–7.
35. Utsunomiya T, Saitsu H, Saku M, Yoshida K, Matsumata T, Shimada M, et al. Rare occurrence of colorectal cancer metastasis in livers infected with hepatitis B or C virus. *Am J Surg* 1999;177:279–81.
36. Della Chiesa M, Falco M, Muccio L, Bertaina A, Locatelli F, Moretta A. Impact of HCMV infection on NK cell development and function after HSCT. *Front Immunol* 2013;4:458.
37. Green ML, Leisenring WM, Xie H, Walter RB, Mielcarek M, Sandmaier BM, et al. CMV reactivation after allogeneic HCT and relapse risk: evidence for early protection in acute myeloid leukemia. *Blood* 2013;122:1316–24.
38. Gotte M, Feld JJ. Direct-acting antiviral agents for hepatitis C: structural and mechanistic insights. *Nat Rev Gastroenterol Hepatol* 2016;13:338–51.
39. Reig M, Marino Z, Perello C, Inarrairaegui M, Ribeiro A, Lens S, et al. Unexpected high rate of early tumor recurrence in patients with HCV-related HCC undergoing interferon-free therapy. *J Hepatol* 2016;65:719–26.
40. Conti F, Buonfiglioli F, Scuteri A, Crespi C, Bolondi L, Caraceni P, et al. Early occurrence and recurrence of hepatocellular carcinoma in HCV-related cirrhosis treated with direct-acting antivirals. *J Hepatol* 2016;65:727–33.
41. ANRS Collaborative Study Group on Hepatocellular Carcinoma. Lack of evidence of an effect of direct-acting antivirals on the recurrence of hepatocellular carcinoma: data from three ANRS cohorts. *J Hepatol* 2016;65:734–40.
42. Nault JC, Colombo M. Hepatocellular carcinoma and direct acting antiviral treatments: controversy after the revolution. *J Hepatol* 2016;65:663–5.
43. Carrat F, Nahon P, Duclos-Vallee JC, Pageaux GP, Fontaine H, Pol S, et al. Reply to "A strong message is needed to address the issue of HCC recurrence after DAA therapy". *J Hepatol* 2016;65:1269–70.
44. Meissner EG, Wu D, Osinusi A, Bon D, Virtaneva K, Sturdevant D, et al. Endogenous intrahepatic IFNs and association with IFN-free HCV treatment outcome. *J Clin Invest* 2014;124:3352–63.
45. Serti E, Chepa-Lotrea X, Kim YJ, Keane M, Fryzek N, Liang TJ, et al. Successful interferon-free therapy of chronic hepatitis C virus infection normalizes natural killer cell function. *Gastroenterology* 2015;149:190–200e2.
46. Spaan M, van Oord G, Kreeft K, Hou J, Hansen BE, Janssen HL, et al. Immunological analysis during interferon-free therapy for chronic hepatitis C virus infection reveals modulation of the natural killer cell compartment. *J Infect Dis* 2016;213:216–23.
47. Kalkavan H, Sharma P, Kasper S, Helfrich I, Pandya AA, Gassa A, et al. Spatiotemporally restricted arenavirus replication induces immune surveillance and type I interferon-dependent tumour regression. *Nat Commun* 2017;8:14447.
48. Benci JL, Xu B, Qiu Y, Wu TJ, Dada H, Twyman-Saint Victor C, et al. Tumor interferon signaling regulates a multigenic resistance program to immune checkpoint blockade. *Cell* 2016;167:1540–54.e12.
49. Domogala A, Madrigal JA, Saudemont A. Natural killer cell immunotherapy: from bench to bedside. *Front Immunol* 2015;6:264.
50. Zitvogel L, Galluzzi L, Kepp O, Smyth MJ, Kroemer G. Type I interferons in anticancer immunity. *Nat Rev Immunol* 2015;15:405–14.

Cancer Immunology Research

Sustained Type I Interferon Reinforces NK Cell–Mediated Cancer Immunosurveillance during Chronic Virus Infection

Ji Hoon Oh, Myeong Joon Kim, Seong Jin Choi, et al.

Cancer Immunol Res 2019;7:584-599. Published OnlineFirst February 26, 2019.

Updated version Access the most recent version of this article at:
doi:[10.1158/2326-6066.CIR-18-0403](https://doi.org/10.1158/2326-6066.CIR-18-0403)

Supplementary Material Access the most recent supplemental material at:
<http://cancerimmunolres.aacrjournals.org/content/suppl/2019/02/26/2326-6066.CIR-18-0403.DC1>

Cited articles This article cites 49 articles, 15 of which you can access for free at:
<http://cancerimmunolres.aacrjournals.org/content/7/4/584.full#ref-list-1>

E-mail alerts [Sign up to receive free email-alerts](#) related to this article or journal.

Reprints and Subscriptions To order reprints of this article or to subscribe to the journal, contact the AACR Publications Department at pubs@aacr.org.

Permissions To request permission to re-use all or part of this article, use this link
<http://cancerimmunolres.aacrjournals.org/content/7/4/584>.
Click on "Request Permissions" which will take you to the Copyright Clearance Center's (CCC) Rightslink site.